Adv Compos Hybrid Mater
DOI 10.1007/s42114-017-0003-4

BRIEF COMMUNICATION

Significantly enhanced energy density of magnetite/polypyrrole nanocomposite capacitors at high rates by low magnetic fields

Huige Wei[1,2] · Hongbo Gu[3] · Jiang Guo[2] · Dapeng Cui[4] · Xingru Yan[2] · Jiurong Liu[5] · Dapeng Cao[6] · Xuefeng Wang[3] · Suying Wei[7] · Zhanhu Guo[2]

Received: 3 April 2017 / Revised: 27 April 2017 / Accepted: 6 May 2017

Abstract One great challenge existing in electrochemical capacitors (ECs) is to achieve high energy densities at high rates. Currently, most research efforts are focused on development of new electrode materials or modification of the microstructure of traditional electrode materials. Herein, we propose a new strategy for significant enhancement of the energy density of ECs at high rates, in which an external magnetic field is exerted. Results indicate that exertion of a magnetic field can increase the energy density of nanocomposite capacitors significantly. In particular, the energy densities of the magnetite/polypyrrole nanocomposite capacitors containing different content magnetite nanoparticles achieve an increase of more than 10 times at a high current density of 10 A/g, compared to the counterparts without a magnetic field. The possible mechanism is that the magnetic field induces electrolyte ion movement enhancement and charge transfer resistance reduction, which remarkably cause the increase of capacitance and energy density. This work provides an innovative strategy to significantly enhance the rate capabilities of current ECs by a simple physical process rather than chemical process.

Keywords Electrochemical capacitors · Energy density · High rates · Magnetic field

1 Introduction

Sustainable energy reservoirs such as wind, solar` and tides are in urgent demand due to the increasing energy crisis arising

Huige Wei, Hongbo Gu and Jiang Guo contributed equally to this work.

Electronic supplementary material The online version of this article (https://doi.org/10.1007/s42114-017-0003-4) contains supplementary material, which is available to authorized users.

✉ Dapeng Cao
caodp@mail.buct.edu.cn

✉ Zhanhu Guo
zguo10@utk.edu

[1] College of Chemical Engineering and Materials Science, Tianjin University of Science and Technology, Tianjin 300457, China

[2] Integrated Composites Laboratory, Department of Chemical and Biomolecular Engineering, University of Tennessee, Knoxville, TN 37996, USA

[3] Shanghai Key Lab of Chemical Assessment and Sustainability, School of Chemical Science and Engineering, Tongji University, Shanghai 200092, China

[4] College of Packing and Printing Engineering, Tianjin University of Science and Technology, Tianjinx 300222, China

[5] Key Laboratory for Liquid–Solid Structural Evolution and Processing of Materials, Ministry of Education and School of Materials Science and Engineering, Shandong University, Jinan, Shandong 250061, China

[6] State Key Laboratory of Organic–Inorganic Composites, Beijing University of Chemical Technology, Beijing 100029, China

[7] Department of Chemistry and Biochemistry, Lamar University, Beaumont, TX 77710, USA

Published online: 12 October 2017

from the limited reserves of fossil fuels [1–5]. Electrochemical energy storage (EES) systems including batteries, electrochemical capacitors (ECs), and fuel cells are critically needed to store these transient and unstable energies and release them in a stable manner [6–10]. As a key member of EES, ECs have attracted tremendous attention due to their advantages of high power density, exceptional long cycling life, and reliability [11–14].

The electrode materials, which is a key component of ECs [15], generally fall into three categories: (1) porous carbons with high specific surface area (e.g., metal–organic frameworks-derived nanoporous carbon [16, 17], carbide-derived carbon [18], carbon nanotubes [19], graphene [20]), (2) intrinsically conductive polymers (ICPs, e.g., polyaniline [21–23], polypyrrole [24, 25], poly(DNTD) [26, 27]), and (3) transition metal oxides/hydroxides (e.g., RuO_2 [28], MnO_2 [29], MoS_2 [30], $Ni(OH)_2$ [31], $Co(OH)_2$ [32]). Generally, porous carbons serve as electrode materials of electric double-layer capacitors (EDLCs) to store energy via an electrostatic charge accumulation [33], while the ICPs and transition metal oxides/hydroxides serve as electrode materials of pseudocapacitors to store energy via redox reactions [34]. Actually, ICPs and their composites have received ever increasing attention because of their low cost, environmental friendliness, good redox reversibility, and high pseudocapacitance values [35, 36].

One great challenge that ECs faced with is their low energy density compared to batteries (e.g., less than 10 Wh/kg for commercialized ECs vs. 180 Wh/kg for lithium-ion batteries (LIB)), especially at high rates [37, 38]. This challenge originates from the slow transportation of counter ions, which cannot rapidly compensate those consumed in the oxidation-reduction process at higher scan rate or current densities. In addition, the utilization efficiency of electrode materials will be severely compromised at higher rates, and only relatively large pores can be entered by counter ions [39]. To solve the issue, great efforts have been dedicated to fabricating nanostructured electrode materials with larger specific surface area [40] or shorter diffusion path [41]. Unfortunately, there exist still some problems, like the increased undesirable reactions at the electrode/electrolyte interface due to the high specific surface area, and reduced electrical conductivities compared to those of their bulk counterparts due to the shortened electron mean free path arising predominantly from the surface scattering in the nanomaterials [42]. More recently, Juliette [43] et al. found that using low external magnetic field can produce high-rate LIB graphite anodes with an out-of-plane aligned architecture. The magnetically responsive graphite flakes coated by Fe_3O_4 could align perpendicularly to the current collector paths by the magnetic field in the electrode fabrication, and therefore reduce the diffusion path and expose preferential insertion/extraction sites for Li^+. Motivated by the observation above, herein, we propose a new magnetic field exertion strategy to enhance the energy density of nanocomposite ECs at high rates. In particular, by exerting a low magnetic field on the capacitors, the energy densities of magnetite/polypyrrole (Fe_3O_4/PPy) nanocomposite capacitors containing 10.0, 20.0, and 40.0 wt% Fe_3O_4 nanoparticles gain an increase of more than 10 times at a high current density of 10 A/g, compared to the counterparts without a magnetic field.

2 Experiment

2.1 Fabrication of Fe_3O_4/PPy nanocomposites

Fe_3O_4/PPy nanocomposites were synthesized using a facile surface initiated polymerization method as reported before [44]. Briefly, magnetite nanoparticles with a size of 12 nm (Nanjing Emperor Nano Material Co., Ltd., 99.5%) were dispersed in 100-mL deionized water containing 15 mmol *p*-toluene sulfonic acid ($C_7H_8O_3S$, Sigma-Aldrich, ≥ 98.5%) and 9 mmol ammonium persulfate ($(NH_4)_2S_2O_8$, Sigma-Aldrich, 98%) under sonication and mechanical stirring for 1 h in an ice-water bath. Then, 18 mmol pyrrole monomers (C_4H_5N, Sigma-Aldrich, ≥ 98%) in 25 mL deionized water were mixed with the above magnetite nanoparticle suspension, and the mixture was mechanically and ultrasonically stirred for another one and a half hours for a complete polymerization of the monomers. The product was filtered and rinsed with around 250 mL deionized water. The precipitant was further washed with 1.0 M *p*-toluene sulfonic acid. The final nanocomposites were dried at 60 °C overnight in a traditional oven. The pure PPy and its magnetite nanocomposites with an initial loading of 10.0, 20.0, 40.0 wt% magnetite nanoparticles were synthesized and denoted as PPy, M-10.0, M-20.0, and M-40.0, respectively.

2.2 Characterizations of Fe_3O_4/PPy nanocomposites

Bruker Inc. Vector 22 coupled with an ATR accessory was used to obtain the Fourier transform infrared (FT-IR) spectra of the Fe_3O_4/PPy nanocomposites over the range of 500 to 2200 cm^{-1} at a resolution of 4 cm^{-1}. Thermogravimetric analysis (TGA) was operated on a TGA Q-500 and heated from 25 to 700 °C at a heating rate of 10 °C min^{-1} under an air-flow rate of 60 mL min^{-1}. The scanning electron microscope (SEM) of the samples coated with carbon was performed on a JEOL JSM-6510LV system. The high-resolution transmission electron microscope (HRTEM) was performed on the Hitachi H9000NAR. The electrical resistivity was measured by a standard four-probe method.

2.3 Preparation of Fe_3O_4/PPy nanocomposite electrodes

About 1-mg Fe_3O_4/PPy nanocomposites with different loadings of magnetite nanoparticles were weighed using UMX2 ultra-microbalance and pressed uniformly onto a PELCO

Tabs™ double-coated carbon conductive tape (6 mm OD), which was adhered to a carbon paper substrate. Each sample was weighed for five times to obtain an average value within a deviation of ± 3%.

2.4 Electrochemical property measurements

The electrochemical properties including cyclic voltammetry, galvanostatic charge-discharge measurements, and electrochemical impedance spectroscopy techniques were performed on an electrochemical working station VersaSTAT 4 potentiostat (Princeton Applied Research). A typical electrochemical cell consisting of a reference electrode, a working electrode, and a counter electrode was employed. A saturated calomel electrode (SCE) served as the reference electrode and a platinum (Pt) wire as the counter electrode. The CV was scanned from − 0.2 to 0.8 V vs. SCE at a series of scan rates in 1.0 M H_2SO_4 (Sigma-Aldrich, 95.0–98.0%) aqueous solution, and the CV curve in the second cycle was taken. EIS was carried out in the frequency range from 100,000 to 0.01 Hz at a 5 mV amplitude referring to the open circuit potential. The stability of the nanocomposites was also assessed using charge-discharge measurements at a current density of 10 A/g. To study the effects of magnetic field on the electrochemical performance, the whole electrochemical cell was fixed in a field of 0.1 T, generating between two magnetic poles of an electromagnet (EM4-HVA H-Yoke, Lake ShoreCryotronics, Inc. USA), Scheme 1a.

3 Results and discussion

3.1 Structure and morphology characterization

The SEM (Fig. S1) reveals the particulate structure of Fe_3O_4/PPy nanocomposites with a fairly uniform size distribution. The HRTEM image (Fig. 1a) shows that the nanocomposites exhibit a core-shell structure where crystalline magnetite nanoparticles (Fig. 1b) are coated by an amorphous PPy polymer layer. The acid dissolution result further proves the integrity of the core-shell structure since the core of magnetite nanoparticles could not be dissolved in the strong acid. The peak shifts in the FTIR spectroscopy (Fig. 1c) results indicate interactions between the magnetite nanoparticles and the PPy polymer matrix. Higher decomposition temperatures at 10.0% weight loss from TGA curves (254, 257, 272, 287 °C for PPy, M-10.0, M-20.0, M-40.0, respectively, Fig. 1d) implies an enhanced thermal stability of the magnetite nanocomposites. The electrical conductivity test (Fig. S2) shows that the conductivity of the magnetite nanocomposites decrease with increasing the loadings of magnetite nanoparticles, which is reasonable for the semiconducting nature of magnetite nanoparticles.

3.2 Cyclic voltammetry

The effects of magnetic fields on the electrochemical properties of pure PPy and its magnetite nanocomposites were investigated using cyclic voltammetry (CV), galvanostatic

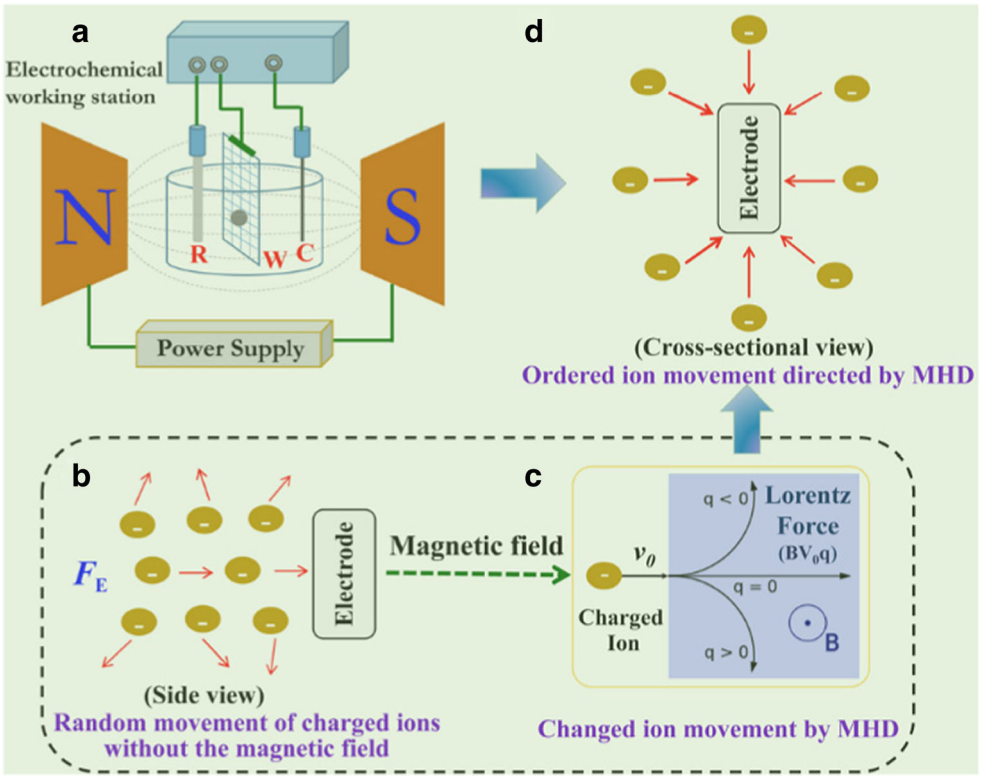

Scheme 1 **a** Experiment setup for conducting the electrochemical measurement under the magnetic field (the intensity is 0.1 T). **b** The random movement of charged ions without the magnetic field. **c** Changed movement of charged electrolyte ions with the magnetic field. **d** Ordered ion movement directed by MHD

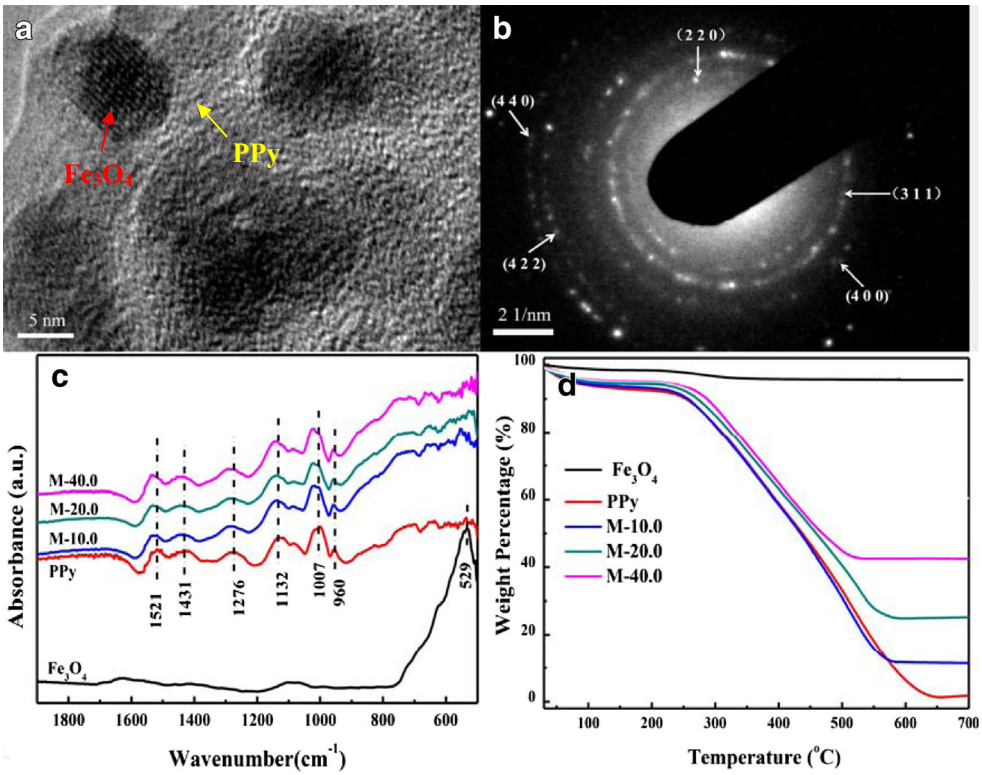

Fig. 1 **a** HRTEM images of the Fe_3O_4/PPy nanocomposite with a magnetite nanoparticle loading of 40 wt%. **b** The corresponding selected area electron diffraction (SAED) of the magnetite. **c** FT-IR spectra. **d** TGA curves of the magnetite nanoparticles, pure PPy, and its nanocomposites

charge-discharge (GCD), and electrochemical impedance spectroscopy using a three-electrode setup in 1.0 M H_2SO_4 aqueous solution. To apply an external magnetic field to the electrode, the whole electrochemical cell was fixed between two magnetic poles of an electromagnet, where the current was parallel to the applied magnetic field (0.1 T), as shown in Scheme 1a. CV measurements with and without the magnetic fields were carried out at different scan rates (200, 100, 50, 20, and 10 mV/s, Fig. S3 and S4). As shown in Fig. 2a, at the case of 200 mV/s without the magnetic field, the pure PPy exhibits Faradic currents without obvious redox peaks in the potential range from − 0.2 to 0.8 V, whereas a pair of redox peaks (oxidation peak "I" at around 0.5 V in the positive scan and the reduction peak "I′" at around 0.3 V in the negative scan) associated with the magnetite nanoparticles [45] is observed in the nanocomposites; the peak current density becomes much higher with increasing the nanoparticle loading. A positive shift from 0.46 to 0.52 V in the oxidation peak and a negative shift from 0.36 to 0.31 V in the corresponding reduction peak are also noted with increasing the nanoparticle loading from 20.0 to 40.0 wt%. The FTIR results (Fig. 1c) confirm that the interactions of the coordinate bonds formed between the lone pair electrons of the nitrogen atom in PPy and the 3d orbital of the iron atom [46, 47] are responsible for the redox potential shifts. Higher current densities are observed in PPy and its magnetite nanocomposites under the magnetic field, as shown in

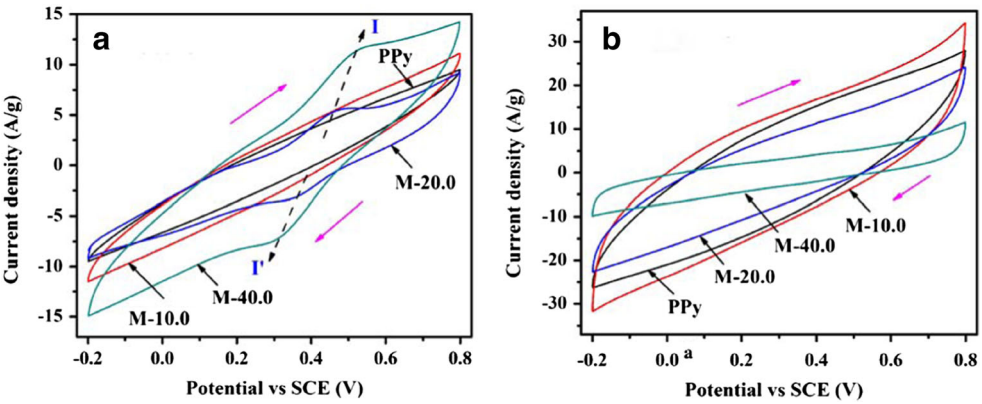

Fig. 2 CV curves of pure PPy and its magnetite nanocomposites with different particle loadings in the **a** absence and **b** presence of the magnetic field at a scan rate of 200 mV/s under a potential range from − 0.2 to 0.8 V in 1.0 M H_2SO_4 aqueous solution

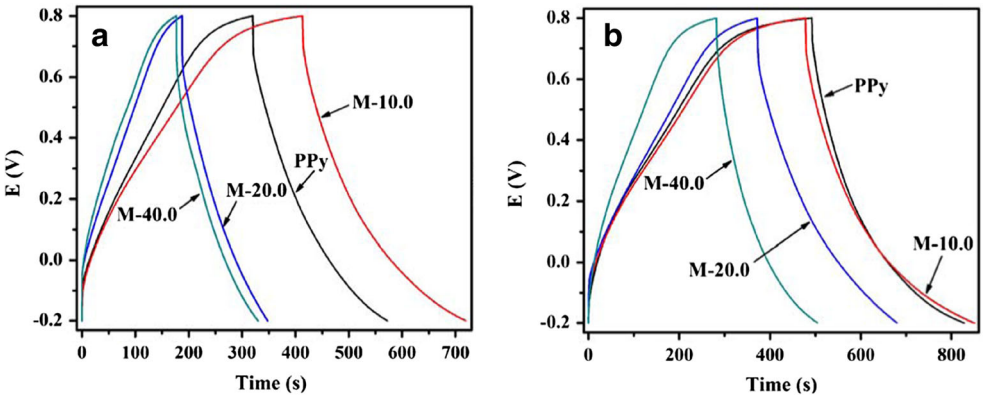

Fig. 3 Galvanostatic charge-discharge curves of pure PPy and its magnetite nanocomposites with different particle loadings without (**a**) and with (**b**) a magnetic field at 1.0 A/g in a 1.0 M H_2SO_4 aqueous solution

Fig. 2b, which suggests that the magnetic field is capable of inducing more energy stored in the electrode material. It is also worth noting that the redox peaks stemming from the redox reactions of magnetite nanoparticles in the nanocomposites disappear upon applying the magnetic field. This phenomenon is inferred to be caused by the "half-metallic" ferromagnetic nature of magnetite, where both the metallic nature for one electron spin and the insulating nature for the other coexist in the magnetite [48]. The metallic electron spin of the magnetite aligns along the magnetic direction upon exposure to the external field and flows easily via the coordinate bond to the PPy matrix, and therefore, no redox peaks could be observed.

3.3 Galvanostatic charge-discharge measurement

The galvanostatic charge-discharge (GCD) measurements under conditions with and without the magnetic fields were performed at different current densities (10, 5, 3, 2, and 1 A/g, Fig. S5 and S6) to obtain the specific capacitance of pure PPy and its magnetite nanocomposites. The corresponding specific capacitances at different current densities are calculated according to Eq. S1 in Supporting Information. Interestingly, the magnetic fields induce the significant improvement of the specific capacitances of all the nanocomposites (Table S1). For the 10.0 wt% magnetite nanocomposite, the capacitance is increased by 126.8% at a current density of 10 A/g. Less remarkable enhancement was observed at lower current densities, which is similar to what was observed by Juliette [43] et al. in the LIB graphite anodes. However, the 10.0 wt% magnetite nanocomposite still wins 24.3% increase in the specific capacitance, from 332.9 (Fig. 3a, without the magnetic field) to 413.8 F/g (Fig. 3b, with the magnetic field) even at a low current density of 1.0 A/g, implying a higher energy storage capability of the electrode under the magnetic field.

Figure 4 presents the Ragone plots of pure PPy and its magnetite nanocomposites with and without the magnetic fields. The energy density (E) and power density (P) (Table S2) calculated from Eq. S2 and S3, respectively, are increased by a factor of 10.5 and 2.2, 11.1 and 1.4, 19.3 and 1.5, for the composites with a nanoparticle loading of 10.0, 20.0, and 40.0 wt%, respectively, at a current density of 10 A/g. Therefore, it suggests that the magnetic field significantly improves the energy storage capabilities and does not sacrifice their high power densities.

3.4 Electrochemical impedance spectroscopy

Electrochemical impedance spectroscopy (EIS) was employed to unveil the behind mechanisms governing the magnetic field induced electrochemical performance enhancement. Figure 5 shows the EIS spectra under both conditions (with and without the magnetic fields), in which the

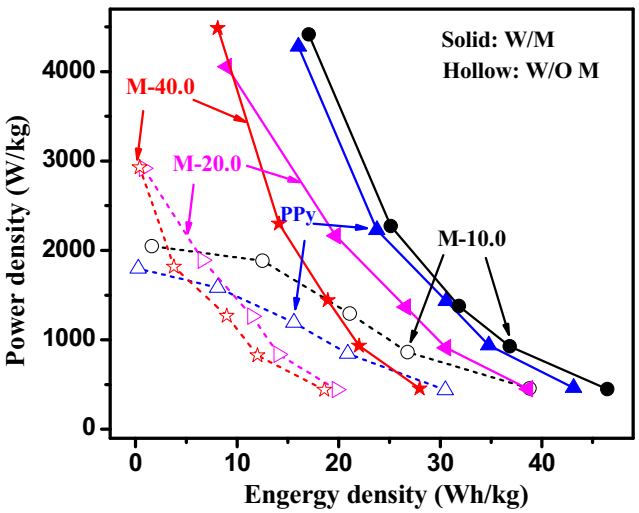

Fig. 4 Ragone plot of pure PPy and its magnetite composites at different current densities under a potential range of − 0.2 to 0.8 V in 1.0 M H_2SO_4 aqueous solution in the absence and presence of the external magnetic field. W/O M denotes no magnetic field and W/M denotes with magnetic field

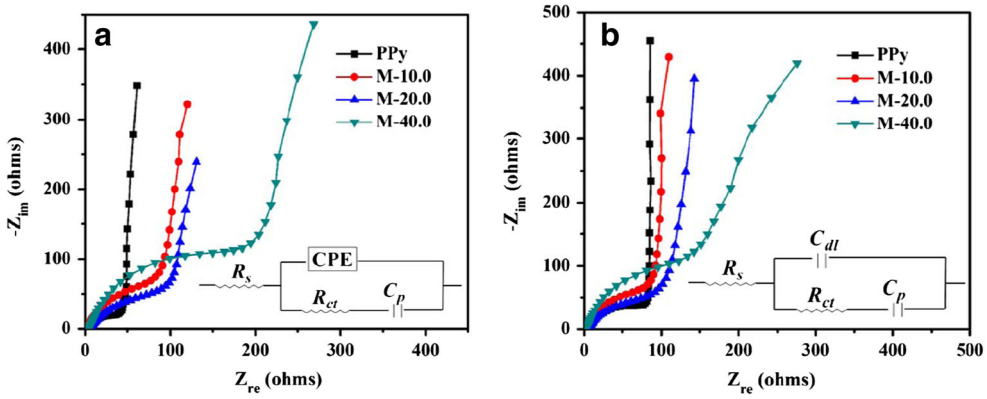

Fig. 5 Nyquist plots of pure PPy and its magnetite nanocomposites with different particle loadings in the **a** absence and **b** presence of an external magnetic field. Inset is the corresponding equivalent circuit

nanocomposites exhibit a semicircle at higher frequency region representing a charge transfer resistance (or Faraday resitance, R_{ct}), and a straight line at lower frequency region indicating a capacitive behavior [49]. Considering the electrochemical processes in the cell, an equivalent circuit was proposed and the values of the elements were fitted using ZsimpWin software. The equivalent circuit consists of the equivalent series resistance (R_s, mainly arising from the electrolyte, the intrinsic resistance of the active material, and the contact resistance at the active material/current collector interface), R_{ct}, the resistance at the electrolyte/electrode interface, the double layer capactiance at the electrode/electrolyte interface (C_{dl}), and the pseudocapacitance (C_p) in the nanocomposites, respectively [38]. A constant phase element (CPE) defined by Eq. S4 [50] is employed in the equivalent circuit considering the deviation from the ideal capacitor behavior. Without the magnetic field, the composite electrode in Fig. 5a exhibits a much higher capacitance from C_p than C_{dl} or CPE (Table S3), suggesting a main contribution from the pseudocapacitors. In addition, R_{ct} generally increases with the increase in the magnetite nanoparticle loading, which is consistent with the poor conductive nature of the magnetite nanoparticles [51]. A great decreament in R_{ct} for the pure PPy and its magnetic nanocomposite electrodes is observed upon applying a magnetic field (Table S4), as shown in Fig. 5b. It is also noted that the ion diffusion coefficient (D) calculated from the EIS data (Eq. S5 and 6) in the low frequency region [52] (< 1 Hz) was increased by applying a magnetic field. For example, in the nanocomposites with 10.0 wt% nanoparticles, D was enhanced from 3.81×10^{-9} to 9.24×10^{-9} cm^2/s when exposed to the magnetic field (Fig. 6).

3.5 Mechanism of magnetic field-enhanced electrochemical performance

Based on the EIS analysis, the mechanism of the magnetic field-enhanced electrochemical performance is proposed and shown in Scheme 1b–d. In the condition without a magnetic field, the charged electrolyte ions moved randomly. The ions moving parallel to the electrical field get accelerated by the electrostatic force, F_E, and diffuse faster toward the electrode materials to participate in the redox reactions. For those moving perpendicular to the electrical field, it may take longer for their moving direction to be changed via collisions with other ions or may never reach the electrode material, as illustrated in Scheme 1b. Upon applying a magnetic field, the movement of the former is not affected. However, the dynamic motion of the latter can be altered by the Lorentz force in the magnetic field, and then get accelerated under a combined effect of the electrostatic force and the Lorentz force (magnetohydrodynamics effect, MHD), as shown in Scheme 1c. The faster-moving ions are capable of getting accessible to the electrode surfaces much more efficiently to compensate the ions consumed by the redox reactions in the electrode materials, as shown in Scheme 1d, which leads to an enhanced ion movement and reduces R_{ct}, and therefore gives rise to an increased capacitance, and ultimately larger energy densities (Eq. S7). Since the combination of the electrostatic and the Lorentz forces increases with increasing the current density, it can be

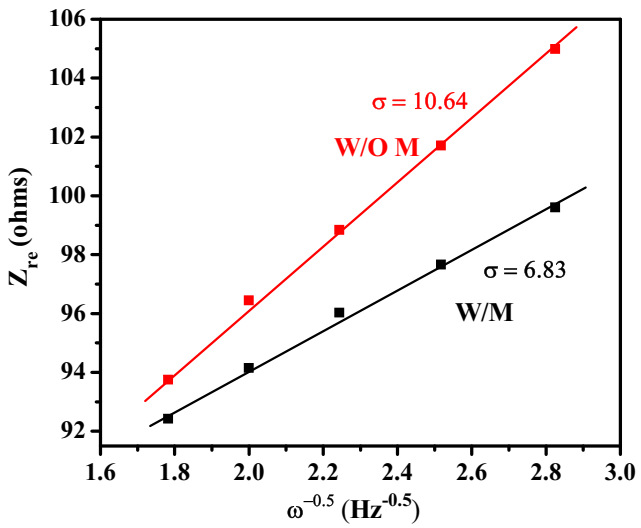

Fig. 6 The Warburg factor σ with and without the magnetic field in the nanocomposites with 10.0 wt% magnetite nanoparticles can be calculated from the slopes of Z_{re} vs. $\omega^{-0.5}$ in the low frequency region (< 1 Hz)

inferred that the magnetic field is much more effective in enhancing the energy densities at higher rates, and therefore improving the rate capabilities of ECs.

4 Conclusions

In summary, we have demonstrated that the magnetic field can significantly enhance the energy densities of magnetite/polypyrrole nanocomposite electrodes at high rates. The combined force under the electric and magnetic fields increased the specific capacitance, and therefore attributed to enlarged energy densities through the manipulation of the dynamic motion of the electrolyte ions and the reduction of the charge transfer resistance. The magnetic field increased the energy density by a factor of 10.5, 11.1, and 19.3, at a high current density of 10 A/g for the magnetite/polypyrrole nanocomposite electrodes at a magnetite particle loading of 10.0, 20.0, and 40.0 wt%, respectively. This simple approach provides an innovative alternative to significantly enhancing the energy density of ECs at high rates without compromising their power densities and is envisioned to influence other storage units such as LIBs and fuel cells as well.

Acknowledgements This work is financially supported by National Science Foundation–Nanomanufacturing (Grant Number: CMMI-13–14486); Nanoscale Interdisciplinary Research Team and Materials Processing and Manufacturing (Grant Number: CMMI 10–30755); Tianjin Natural Science Foundation (Grant Number: 1600030041). D. C. is thankful for National Science Fund for Distinguished Young Scholars (No. 21625601).

References

1. Wang S, Wang ZL, Yang Y (2016) A one-structure-based hybridized nanogenerator for scavenging mechanical and thermal energies by triboelectric-piezoelectric-pyroelectric effects. Adv Mater 28: 2881–2887
2. Xu B, Bi D, Hua Y, Liu P, Cheng M, Grätzel M, Kloo L, Hagfeldt A, Sun L (2016) A low-cost spiro[fluorene-9,9′-xanthene]-based hole transport material for highly efficient solid-state dye-sensitized solar cells and perovskite solar cells. Energy Environ Sci 9:873–877
3. Li Y, Meng L, Yang Y, Xu G, Hong Z, Chen Q, You J, Li G, Yang Y, Li Y (2016) High-efficiency robust perovskite solar cells on ultrathin flexible substrates. Nat Commun 7:10214
4. Gao L, Zhang ZG, Bin H, Xue L, Yang Y, Wang C, Liu F, Russell TP, Li Y (2016) High-efficiency nonfullerene polymer solar cells with medium bandgap polymer donor and narrow bandgap organic semiconductor acceptor. Adv Mater 28:8288–8295
5. Guo H, Li T, Cao X, Xiong J, Jie Y, Willander M, Cao X, Wang N, Wang ZL (2017) Self-sterilized flexible single-electrode triboelectric nanogenerator for energy harvesting and dynamic force sensing. ACS Nano 11:856–864
6. Ye Z, Wang L, Guo Z, Xu Y, Wang Y, Peng H (2016) High-performance lithium–air battery with a coaxial-fiber architecture. Angew Chem Int Ed 55:4487–4491
7. Yu D, Qian Q, Wei L, Jiang W, Goh K, Wei J, Zhang J, Chen Y (2015) Emergence of fiber supercapacitors. Chem Soc Rev 44:647–662
8. Irvine JTS, Neagu D, Verbraeken MC, Chatzichristodoulou C, Graves C, Mogensen MB (2016) Evolution of the electrochemical interface in high-temperature fuel cells and electrolysers. Nature Energy 1:15014
9. Xiang Z, Cao D, Huang L, Shui J, Wang M, Dai L (2014) Nitrogen-doped holey graphitic carbon from 2D covalent organic polymers for oxygen reduction. Adv Mater 26:3315–3320
10. Xiang Z, Xue Y, Cao D, Huang L, Chen JF, Dai L (2014) Highly efficient electrocatalysts for oxygen reduction based on 2D covalent organic polymers complexed with non-precious metals. Angew Chem Int Ed 53:2433–2437
11. Ramadoss A, Saravanakumar B, Lee SW, Kim YS, Kim SJ, Wang ZL (2015) Piezoelectric-driven self-charging supercapacitor power cell. ACS Nano 9:4337–4345
12. Song R, Jin H, Li X, Fei L, Zhao Y, Huang H, Chan LW, Wang Y, Chai Y (2015) A rectification-free piezo-supercapacitor with a polyvinylidene fluoride separator and functionalized carbon cloth electrodes. J Mater Chem A 3:14963–14970
13. Huang P, Lethien C, Pinaud S, Brousse K, Laloo R, Turq V, Respaud M, Demortière A, Daffos B, Taberna PL (2016) On-chip and freestanding elastic carbon films for micro-supercapacitors. Science 351:691–695
14. Muller GA, Cook JB, Kim HS, Tolbert SH, Dunn B (2015) High performance pseudocapacitor based on 2D layered metal chalcogenide nanocrystals. Nano Lett 15:1911–1917
15. Wang G, Zhang L, Zhang J (2012) A review of electrode materials for electrochemical supercapacitors. Chem Soc Rev 41:797–828
16. Zhong S, Zhan C, Cao D (2015) Zeolitic imidazolate framework-derived nitrogen-doped porous carbons as high performance supercapacitor electrode materials. Carbon 85:51–59
17. Zhang P, Sun F, Shen Z, Cao D (2014) ZIF-derived porous carbon: a promising supercapacitor electrode material. J Mater Chem A 2: 12873–12880
18. Dyatkin B, Gogotsi O, Malinovskiy B, Zozulya Y, Simon P, Gogotsi Y (2016) High capacitance of coarse-grained carbide derived carbon electrodes. J Power Sources 306:32–41
19. Yu J, Lu W, Pei S, Ke G, Wang L, Meng L, Huang Y, Smith JP, Booksh KS, Li Q (2016) Omnidirectionally stretchable high-performance supercapacitor based on isotropic buckled carbon nanotube films. ACS Nano 10:5204–5211
20. Zhu J, Childress AS, Karakaya M, Dandeliya S, Srivastava A, Lin Y, Rao AM, Podila R (2016) Defect-engineered graphene for high-energy-and high-power-density supercapacitor devices. Adv Mater 28:7185–7192
21. Wei H, Yan X, Wu S, Luo Z, Wei S, Guo Z (2012) Electropolymerized polyaniline stabilized tungsten oxide nanocomposite films: electrochromic behavior and electrochemical energy storage. J Phys Chem C 116:25052–25064
22. Wei JZH, Wu S, Wei S, Guo Z (2013) Electrochromic polyaniline/graphite oxide nanocomposites with endured electrochemical energy storage. Polymer 54:1820–1831
23. Wei H, Guo J, Wei S, Guo Z (2013) Electropolymerized polyaniline nanocomposites from multi-walled carbon nanotubes with tuned surface functionalities for electrochemical energy storage. J Electrochem Soc 160:G3038–G3045
24. Yang C, Wei H, Guan L, Guo J, Wang Y, Yan X, Zhang X, Wei S, Guo Z (2015) Polymer nanocomposites for energy storage, energy saving, and anticorrosion. J Mater Chem A 3:14929–14941
25. Wei H, He C, Liu J, Gu H, Wang Y, Yan X, Guo J, Ding D, Shen NZ, Wang X (2015) Electropolymerized polypyrrole

nanocomposites with cobalt oxide coated on carbon paper for electrochemical energy storage. Polymer 67:192–199
26. Wei H, Yan X, Li Y, Wu S, Wang A, Wei S, Guo Z (2012) Hybrid electrochromic fluorescent poly (DNTD)/CdSe@ZnS composite films. J Phys Chem C 116:4500–4510
27. Wei H, Yan X, Li Y,Gu H, Wu S, Ding K, Wei S, Guo Z (2012) Electrochromic poly (DNTD)/WO_3 nanocomposite films via electorpolymerization. J Phys Chem C 116:16286–16293
28. Krause PP, Camuka H, Leichtweiss T, Over H (2016) Temperature-induced transformation of electrochemically formed hydrous RuO2 layers over Ru(0001) model electrodes. Nano 8:13944–13953
29. Choi C, Sim HJ, Spinks GM, Lepró X, Baughman RH, Kim SJ (2016) Elastomeric and dynamic MnO_2/CNT core–shell structure coiled yarn supercapacitor. Adv Energy Mater 6:1502119–1502126
30. Acerce M, Voiry D, Chhowalla M (2015) Metallic 1T phase MoS_2 nanosheets as supercapacitor electrode materials. Nat Nanotechnol 10:313–318
31. Parveen N, Cho MH (2016) Self-assembled 3D flower-like nickel hydroxide nanostructures and their supercapacitor applications. Sci Rep 6:27318
32. Liu H, Ho KH, Hu Y, Ke Q, Mao L, Zhang Y, Wang J (2015) Doping cobalt hydroxide nanowires for better supercapacitor performance. Acta Mater 84:20–28
33. Griffin JM, Forse AC, Tsai WY, Taberna PL, Simon P, Grey CP (2015) In situ NMR and electrochemical quartz crystal microbalance techniques reveal the structure of the electrical double layer in supercapacitors. Nat Mater 14:812–819
34. Augustyn V, Simon P, Dunn B (2016) Pseudocapacitive oxide materials for high-rate electrochemical energy storage. Energy Environ Sci 7:1597–1614
35. Li W, Gao F, Wang X, Zhang N, Ma M (2016) Strong and robust polyaniline-based supramolecular hydrogels for flexible supercapacitors. Angew Chem Int Ed 128:9342–9347
36. Sun J, Huang Y, Fu C, Wang Z, Huang Y, Zhu M, Zhi C, Hu H (2016) High-performance stretchable yarn supercapacitor based on PPy@CNTs@urethane elastic fiber core spun yarn. Nano Energy 27:230–237
37. Chou TC, Huang CH, Doongn RA, Hu CC (2013) Architectural design of hierarchically ordered porous carbons for high-rate electrochemical capacitors. J Mater Chem A 1:2886–2895
38. Wei H, Gu H, Guo J, Wei S, Liu J, Guo Z (2013) Silica doped nanopolyaniline with endured electrochemical energy storage and the magnetic field effects. J Phys Chem C 117:13000–13010
39. Wang DW, Li F, Liu M, Lu GQ, Cheng HM (2008) 3D aperiodic hierarchical porous graphitic carbon material for high-rate electrochemical capacitive energy storage. Angew Chem 47:373–376
40. Zhu Y, Cui H, Xin M, Zheng J, Yang P, Li L, Wang Z, Jia S, Zhu Z (2016) Chlorine-induced in situ regulation to synthesize graphene frameworks with large specific area for excellent supercapacitor performance. ACS Appl Mater Interfaces 8:6481–6487
41. Yu G, Hu L, Liu N, Wang H, Vosgueritchian M, Yang Y, Cui Y, Bao Z (2011) Enhancing the supercapacitor performance of graphene/MnO_2 nanostructured electrodes by conductive wrapping. Nano Lett 11:4438–4442
42. Barati M, Sadeghi E (2001) Study of the ordinary size effect in the electrical conductivity of Bi nanowires. Nanotechnology 12:277–280
43. Billaud J, Bouville F, Magrini T, Villevieille C, Studart AR (2016) Magnetically aligned graphite electrodes for high-rate performance Li-ion batteries. Nature Energy 1:16097
44. Guo J, Gu H, Wei H, Zhang Q, Haldolaarachchige N, Li Y, Young DP, Wei S, Guo Z (2013) Magnetite–polypyrrole metacomposites: dielectric properties and magnetoresistance behavior. J Phys Chem C 117:10191–10202
45. Radhakrishnan S, Prakash S, Rao CR, Vijayan M (2009) Organically soluble bifunctional polyaniline–magnetite composites for sensing and supercapacitor applications. Electrochem Solid-State Lett 12:A84–A87
46. Deng J, Peng Y, He C, Long X, Li P, Chan AS (2003) Magnetic and conducting Fe_3O_4-polypyrrole nanoparticles with core-shell structure. Polym Int 52:1182–1187
47. Wu TM, Yen SJ, Chen EC, Sung TW, Chiang RK (2007) Conducting and magnetic behaviors of monodispersed iron oxide/polypyrrole nanocomposites synthesized by in situ chemical oxidative polymerization. J Polym Sci A Polym Chem 45:4647–4655
48. Gu XZH, Wei H, Huang Y, Wei S, Guo Z (2013) An overview of the magnetoresistance phenomenon in molecular systems. Chem Soc Rev 42:5907–5943
49. Simon P, Gogotsi Y, Dunn B (2014) Where do batteries end and supercapacitors begin? Science 343:1210–1211
50. Li H, Wang J, Chu Q, Wang Z, Zhang F, Wang S (2009) Theoretical and experimental specific capacitance of polyaniline in sulfuric acid. J Power Sources 190:578–586
51. Karthikeyan K, Kalpana D, Amaresh S, Lee YS (2012) Microwave synthesis of graphene/magnetite composite electrode material for symmetric supercapacitor with superior rate performance. RSC Adv 2:12322–12328
52. Allen LRF, Bard J (2001) Electrochemical methods : fundamentals and applications. Wiley, New York